In Situ Structural Study of MnP$_i$ Modified BiVO$_4$ Photoanodes by Soft X-ray Absorption Spectroscopy

Lifei Xi,[†] Fuxian Wang,[‡] Christoph Schwanke,[†] Fatwa F. Abdi,[‡] Ronny Golnak,[§] Sebastian Fiechter,[‡] Klaus Ellmer,[‡] Roel van de Krol,[‡] and Kathrin M. Lange[†,¦,*]

†Young Investigator Group Operando Characterization of Solar Fuel Materials (EE-NOC), ‡Institute for Solar Fuels, §Institute Methods for Material Development, Helmholtz-Zentrum Berlin für Materialien und Energie GmbH, 12489 Berlin, Germany ¦ Universität Bielefeld, Physikalische Chemie, Universitätsstr.25, D-33615 Bielefeld, Germany.

KEYWORDS. soft XAS, in situ, BiVO$_4$, L-edge, photoanode, photoelectrochemistry, manganese oxide, catalyst, linear combination fitting, reactive magnetron sputtering

ABSTRACT. In this study we demonstrate that the PEC performance of BiVO$_4$ photoanodes can be improved by the deposition of a MnP$_i$ catalyst layer. We investigated the electronic structure of the layer using in situ soft X-ray absorption spectroscopy (XAS) at the Mn L-edge upon varying the applied potentials and the illumination conditions. Using the linear combination method, information on different Mn species and Mn oxidation states were obtained. We found that the charge transfer at the MnP$_i$ / electrolyte interface is affected by band bending related to the applied and the built-in potential. With increasing potential the electronic properties of the MnO$_x$ layer and

its structure are changing, leading to a birnessite-type layer structure associated with an electron transfer from the MnP$_i$ film to the BiVO$_4$ photoanode. The present work should benefit the potential applications of other oxygen evolution catalysts (OECs) on photoanodes.

INTRODUCTION

Photoelectrochemical (PEC) water splitting is a potentially scalable method to store solar energy in the form of renewable hydrogen fuels.[1] The overall water splitting reaction is a thermodynamically uphill reaction (ΔG=237 kJ/mol, equivalent to 1.23 eV) which involves multiple electron transfer processes: the two-electron reduction of water to hydrogen and the four-electron oxidation of water to oxygen.[2] Water oxidation has been recognized as the bottleneck for the water splitting reaction due to the large endothermicity of the reaction.[3]

BiVO$_4$ has recently emerged as one of the most promising photoanode materials for the generation of dioxygen from water due to its favorable optical band gap (~2.4 eV for the monoclinic phase),[4] favorable conduction and valence band edge positions, and relatively high chemical stability in near-neutral aqueous environments. Moreover, it is non-toxic, relatively abundant and can be easily produced on a large scale at low cost.[5] However, without modifications, it suffers from poor electron transport properties and modest catalytic activity. More recently, surface recombination was identified as an even more important performance bottleneck than slow surface reaction kinetics.[6] Loading co-catalysts on BiVO$_4$ photoanodes was previously found to be an effective way to improve the photocurrents and reduce the onset potentials. The investigated co-catalysts include CoO$_x$,[7] cobalt borate (CoB$_i$),[8] cobalt phosphate (CoP$_i$),[9-11] nickel borate (NiB$_i$),[12] nickel bicarbonate (Ni-C$_i$),[13] FeOOH,[14] FeOOH/NiOOH[15] and NiO$_x$.[16] For example, Pilli et al.[9] and Jeon et al.[11] found that photo-deposition of CoP$_i$ onto BiVO$_4$ results in superior performance for water oxidation. In addition, the onset potential shifts favourably (cathodic)

because photo-deposition ensures the selective deposition of CoP_i on the photo-active $BiVO_4$ surface sites. Abdi *et al.* showed an AM1.5 photocurrent of ~1.7 mA cm^{-2} at 1.23 V vs. the reversible hydrogen electrode (RHE) for a CoP_i modified undoped $BiVO_4$ photoanode, more than double that of the pristine $BiVO_4$.[10] Kim *et al.* coupled both FeOOH and NiOOH as dual-layer oxygen evolution reaction (OER) catalyst onto porous undoped $BiVO_4$ electrodes and achieved a photocurrent as high as 2.73 mA cm^{-2} at a potential as low as 0.6 V vs. RHE.[15] Despite these successes, the role of these co-catalysts is not yet fully understood.[4] Co-catalysts may accelerate catalysis of the water oxidation reaction, but could also reduce surface recombination by preventing back-electron transfer or by chemically passivating surface traps.[4,17] Recent work has shown that the performance of spray-deposited $BiVO_4$ is indeed limited by surface recombination, not surface catalysis.[6] Understanding the physical and chemical nature of the semiconductor/electrolyte interface, as well as the electronic structure of co-catalyst under in situ conditions, will help to design more effective semiconductor/catalyst systems.[5]

Manganese oxides (MnO_x) have been widely recognized as promising catalysts for water oxidation.[18,19] The performance of MnO_x catalysts relates to the electronic structure and is affected by the Mn oxidation state, i.e. the Mn-to-O atomic arrangement.[18] The local structure and water oxidation mechanism of MnO_x catalysts have been investigated using ex situ electron paramagnetic resonance (EPR)[20] and hard XAS (X-ray Absorption Near Edge Spectroscopy, XANES and Extended X-ray Absorption Fine Structure spectroscopy, EXAFS)[21] analysis. Very recently, Huynh *et al.* reported an electrodeposited manganese oxide (MnO_x or named as MnP_i in the present study due to the presence of supporting phosphate buffer electrolyte, methylphosphate (MeP_i)) which has considerably high intrinsic and functional kinetic stability in acidic electrolytes due to a Mn^{3+} disproportionation process.[22-24] In the past, acidic stable OER catalysts were

dominated by oxides containing iridium and/or ruthenium,[16] which are expensive and not scalable. The acidic stability of an earth-abundant OER catalyst is therefore highly in demand for the overall water splitting reaction.[1] This makes MnP_i a promising OER catalyst, since it opens up the possibility of a combination with acidic-stable photoanodes, such as the dominating photovoltaic material, silicon.[23] Huynh *et al*. studied the water oxidation mechanism of MnP_i via electrochemical kinetic experiments and obtained structure information using ex situ X-ray photoelectron spectroscopy (XPS), powder X-ray diffraction (XRD), X-ray scattering and pair distribution function (PDF)[23] analysis.

Soft XAS is a powerful element-specific method to probe the partially occupied Mn d-orbitals and to reveal detailed information about oxidation state contributions, spin-states and charge transfer.[25,26] It has been used to study MnO_x films under ex-situ conditions.[18,19,27,28] While these studies are undoubtedly useful, questions arise whether the information is relevant for *in situ* OER conditions. In-situ soft XAS experiments are, however, experimentally highly challenging due to the pressure gap between the soft X-rays required vacuum conditions and the ambient pressure required for the electrolyte solution. The information of the percentage of different Mn oxides under operando conditions as well as metal oxidation state, however, cannot be obtained by X-ray PDF,[23] electrochemistry or ultraviolet and visible (UV-Vis) spectroscopy. In situ near ambient pressure X-ray photoelectron spectroscopy (XPS) is a surface sensitive technique and it can be challenging to obtain reproducible spectra due to the varying thickness of the electrolyte layer and pressure changes within the experimental chamber.[30] Compared to the hard XAS where the transition metal K-edge is probed, soft XAS probes the metal L-edge, which is more favorable for deciphering mixtures of oxidation states due to the narrower natural line widths (Mn K-edge: 1.12 eV; Mn L-edge: 0.32 eV).[29] Thus in order to profit from these advantages of in-situ metal L-edge

XAS we developed an in-situ and operando cell which allows to carry out soft XAS during full electrochemical control over the sample.[31,32]

Recently, we performed an in situ study of electrodeposited MnP_i using soft XAS.[31] The XAS results show that the freshly prepared film at open circuit potential (OCP) contains a dominant contribution of MnO_2 (~75 %) and a contribution from a birnessite-like material (~25%). No or only negligible percentages of MnO, Mn_3O_4 or Mn_2O_3-like Mn species were found in the freshly prepared sample. After 51 min of in situ activation, the birnessite-contribution in the spectrum increased to 75 %. We correlate these changes to the material conversion into an efficient OER catalyst. Although it has been studied as electrocatalyst using soft XAS under operando conditions, it may not necessarily be the same when deposited on a semiconductor. This is the subject of the current study. Here, we demonstrate that the PEC performance of $BiVO_4$ photoanodes can be improved by co-catalyst MnP_i modification. We further investigate the electronic structure information of electrodeposited MnP_i on top of $BiVO_4$ photoanodes using in situ soft XAS. Understanding the electronic structural change under potential, especially during the process of PEC, represents an important step toward gaining a mechanistic understanding of the new emerging catalyst.

EXPERIMENTAL SECTION

Chemicals. Bi (99.9%) and V (99.99%) targets were ordered from FHR Anlagenbau GmbH (Germany). $MnCl_2 \cdot 4H_2O$ (>99.0%), methylphosphoric acid (99.0-101.0%), NaOH (>98%) and KNO_3 (>99.0%) were purchased from Sigma-Aldrich. 50 mM methylphosphate buffer (MeP_i, pH8.0) and 0.1 M potassium phosphate buffer (KP_i, pH7.0) were prepared as described in literature.[22,23,24] KNO_3 was added to maintain ~2 M ionic strength of electrolyte and avoid diffuse double-layer effects.[20] All electrolytes were prepared with DI water (18.6 MΩ.cm). 2 mm x 2mm

x 100 nm Si_3N_4 membrane on Si wafer frames were ordered from Silson Ltd. (UK). Si_3N_4 membranes supported by Si wafers are coated with 1-2 nm Ti and 20 nm gold.

Sputtering $BiVO_4$ Film on FTO or Au/Si_3N_4 Membranes. The $BiVO_4$ films were deposited by reactive magnetron co-sputtering from Bi (99.9%) and V (99.99%) targets at 350 ℃, as reported.[33] The powers of the Bi and the V target were fixed at 40W and 450W, respectively. Before starting the deposition, the substrates were heated to the preset temperature. 6 min deposition yielded a film thickness of approximately 220 nm. After deposition, the films were annealed in air at 500 °C for 2 h in a muffle furnace using a heating ramp of 10 K/min.

Electrodeposition of MnP_i. All electrochemical experiments for deposition, PEC and XAS tests were performed using CHI6016E working station (CHI Instruments) or EmStat3+ (PalmSens) or EG&G Princeton Applied Research 273A potentiostat in a three-electrode system with the $BiVO_4$/FTO or Au/Si_3N_4 substrates as the working electrode, an Ag/AgCl reference electrode and a platinum wire counter electrode inside a home-made electrochemical Teflon cell or beaker. All electrode potentials were converted to the reversible hydrogen electrode (RHE) scale using Nernstian relation: $E_{RHE} = E_{Ag/AgCl} + 0.059 *pH + 0.199V$. For electrodeposition, a freshly prepared nitrogen purged 0.5 mM Mn^{2+} in 50 mM MeP_i buffer solution with added KNO_3. Electrodeposition was carried out at 1.46 V for 1-40 min without stirring and no iR compensation. We found that the maximum photocurrent density is achieved for $BiVO_4$/FTO substrate when the electrodeposition time is 5 min. In order to get a better signal-to-noise ratio, the deposition time for XAS samples has to be extended to around 20 min. After the catalyst deposition, all samples were briefly rinsed with DI water. For comparison, MnP_i was also deposited on FTO/glass or Au/Si_3N_4 substrates. Cyclic voltammetries (CVs) were collected at 50 mV/s in 0.1 M KP_i, pH7.0 electrolyte with 2.0 M KNO_3 added.

Characterization. (a) Morphology and composition test: The morphology and composition of the catalyst on FTO was characterized by FESEM (LEO Gemini 1530). (b) Photoelectrochemical (PEC) test: PEC measurements were performed in a three-electrode configuration in a home-made quartz-windowed Teflon cell. The same Ag/AgCl reference electrode and the platinum counter electrode were used. An AM1.5 solar illumination (100 mWcm^{-2}) with a WACOM super solar simulator (WXS-50S-5H, class AAA) was used as an illumination source. The electrolyte used for all measurements was 0.1 M KP$_i$ buffer solution (pH = 7) with KNO$_3$ added. (c) Differential electrochemical mass spectroscopy (DEMS): The details of the DEMS can be found in previous published works.[34,35] The inlet system between the electrochemical cell and the differential pumped vacuum system of the mass spectrometer (Balzers; QMI 420, QME 125, QMA 125 with 90° off axis SEM) is composed of a porous hydrophobic membrane. The MnP$_i$ modified BiVO$_4$/FTO photoanode is closely attached upside down onto the membrane so that a thin film of the electrolyte between the membrane and the electrode exists which enables the photoelectrochemical experiments. Oxygen formed at the surface of BiVO$_4$/FTO-working electrode surface diffuses through the membrane and can be detected by the mass spectrometer. The reference and counter electrodes are same as above. CV tests under light were carried out in argon-purged 0.1 M KP$_i$ solution with 2.0 M KNO$_3$ added at a scan rate of 2 mV s^{-1}. For the photo-induced reaction the films were illuminated from backside of the working electrode using a Xenon lamp (LXH 100, Müller Elektronik GmbH, Germany). Note: the light intensity is not calibrated to be 1 sun. (d) In situ XAS test: In situ PEC X-ray absorption measurements in transmission mode were performed with a recently developed transmission electrochemical flowcell attached to the LiXEdrom 2.0 endstation at the U56-2 PGM2 beamline at Bessy II. When loading Si$_3$N$_4$ membranes, a Teflon spacer and a gold foil with thickness of 50 -100 μm is added to control the

gap between two membranes. Beam spot is 0.9 x 120-150 μm^2 when a 100 μm exit slit is used. The energy resolution is 186 meV at 640 eV. To avoid a strong background signal induced by the white light LEDs (LEDWE-15, Thorlabs) in transmission measurements a 200 nm thick aluminum film (Lebow Company) was put in front of GaAs photodiode (Hamamatsu G1127). More details can be found in our recent publication.[32] Energy calibration was performed with the 640.3 eV peak using the MnO powder spectrum. The XA spectrum is derived by the logarithm of the transmission, according to the Beer-Lambert law.

$\mu x = - \ln (I_t/I_0)$

where I_t is the transmission signal, I_0 is the mirror current, μ is the absorption coefficient and x is the thickness of the sample. Each Mn L-edge scan takes around 4 min. We averaged 2-5 scans to get better signal-to-noise ratio. The experimental Mn L-edge spectrum was subtracted to the background and then normalized by the integrated area under peaks. (e) Spectra fitting. The experimental spectra are fitted with linear combination fitting method. The percentage values are calculated according to the linear fitting algorithm as below:

Fitted spectrum = a*MnO + b* Mn_3O_4 + c*Mn_2O_3 + d* birnessite + e*MnO_2

Percentage of each manganese oxides is obtained by MnO = a /(a + b + c + d + e), Mn_3O4 = b /(a + b + c + d + e), etc. Here the average oxidation state of 3.7 for birnessite is taken.[36,38]

RESULTS AND DISCUSSION

1. Surface Morphology, Phase and Photoelectrochemical (PEC) Analysis. Figure 1 a and b show SEM images of the $BiVO_4$/FTO/glass photoanodes before and after electrodeposition of MnP_i co-catalyst, respectively (see details of preparation and characterization in the Experimental Section). It can be seen that the morphology of the pristine $BiVO_4$ film is polycrystalline and with a typical lateral big grain size of around 0.5 μm. The film also contains small particles of around

100-200 nm (see Figure S1a). After potentiostatic deposition at 1.46 V (all potentials in this paper are reported with respect to RHE) for 20 min, the BiVO$_4$ photoanode is partially covered by a MnO$_x$ porous layer (see Figure 1b and c). The porous layer contains irregular pores isolated by thin walls (see Figure 1c). This resembles the pedal-like or plate-like features which Huynh *et al.* previously reported for their thick electrodeposited manganese oxide films.[23,24] The morphology of MnP$_i$ on the BiVO$_4$ photoanode differs from that of MnP$_i$ on FTO which showed an amorphous thin film as we previously reported.[31] This difference is most likely due to the different potentials applied for deposition. In the present study, we used 1.46 V while in our previous study 1.05 V vs RHE was used.[31] The reason for using a higher potential is that we found a much slower deposition rate on BiVO$_4$ photoanode compared to FTO. This is probably due to the poorer conductivity of the BiVO$_4$ film compared to the FTO /glass substrate. The X-ray diffraction (XRD) pattern of the BiVO$_4$ film is shown in Figure S2. All diffraction peaks of the BiVO$_4$ film can be correlated to a monoclinic BiVO$_4$ cell (JCPDS no. 14-0668). The composition of film after MnP$_i$ deposition is shown in Figure S1b. The energy-dispersive X-ray spectroscopy (EDS) spectrum and the quantitative results clearly show the presence of Mn but no or only negligible P in the film. However, the presence of phosphate ions during electrodeposition is important because the resulting films deposited in the absence of MeP$_i$ buffer solution are less active and have higher Tafel slopes.[23] The phosphate ions, not being a crucial part of the structure of the catalyst, most likely play an important role as proton-accepting base. Figure 2 shows the PEC activities of the pristine and the MnP$_i$ modified BiVO$_4$/FTO photoanode. It can be seen that the photocurrent is improved after MnP$_i$ modification. Specifically, the photocurrent density of the MnP$_i$ modified BiVO$_4$ photoanode is 0.62 mA cm^{-2} at 1.23 V while that of the pristine is 0.48 mA cm^{-2}, which corresponds to a 29 % improvement. Possible reasons for the photocurrent enhancement are either

surface passivation and/or increasing catalytic activity. Under illumination, the photocurrent onset potential for water oxidation of a MnP$_i$ modified photoanode is around 0.40 V. To ensure that the photocurrent is truly correlated with water oxidation, oxygen gas evolved during cyclic voltammetry (CV) was detected using differential electrochemical mass spectrometry (DEMS) (see Figure S3). It is found that the amount of oxygen gas generated from the MnP$_i$ modified BiVO$_4$ photoanode was increased after MnP$_i$ deposition, which is consistent with our photocurrent improvement.
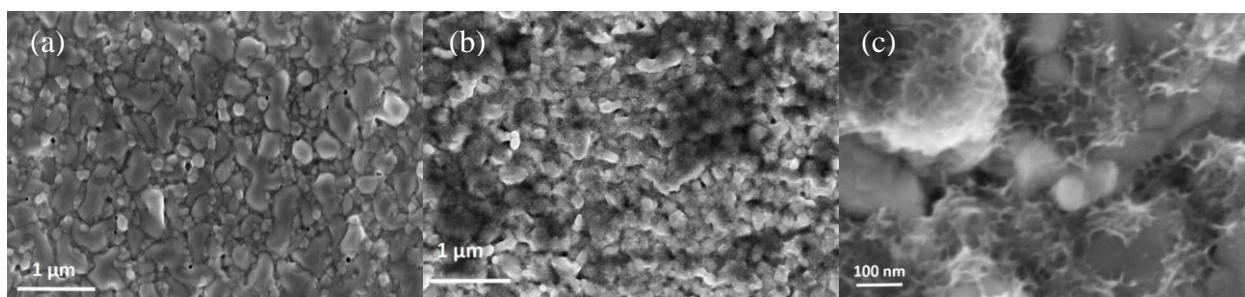

Figure 1. SEM images of the BiVO$_4$/FTO/glass photoanode: (a) before and (b-c) after MnP$_i$ electrodeposition.
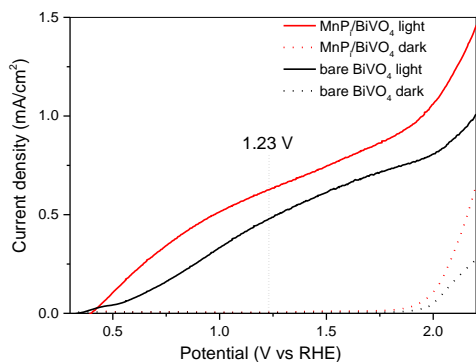

Figure 2. Current–voltage (I–V) curves of BiVO$_4$/FTO photoanodes in 0.1 M KP$_i$ aqueous solution with and without MnP$_i$ modification under dark (dotted lines) and light (solid lines) conditions.

2. In Situ XAS Analysis. In situ XAS measurements were carried out on the MnP$_i$ film deposited on a BiVO$_4$/Au/Si$_3$N$_4$ photoanode under different potentials and illumination conditions in a 0.1

M potassium phosphate (KP$_i$) buffer solution (pH7.0) with 2.0 M KNO$_3$ added (see Figure 3). A pH value of 7.0 was chosen for these measurements due to a better stability of the XAS cell under neutral pH conditions.[32] Under these conditions of X-ray irradiation, white light illumination and applied potential, the MnP$_i$-modified BiVO$_4$ is relatively stable (see Figure S4). It also can be seen that the photocurrent density of photoanode increases when applying a higher potential (1.61 V). Systematic beam damage studies were carried out and measurement times on fresh sample spots were reduced such that the sample damage in the here presented Mn L-edge spectra is considered to be negligible. For detailed analysis previously published manganese oxide reference spectra of MnO (2+), Mn$_3$O$_4$ (2+, 3+), Mn$_2$O$_3$ (3+), birnessite (3+, 4+) and MnO$_2$ (4+) were used and are also shown in Figure 3d and Table S1.[18,19,37] The energetic peak positions and their relative intensities are closely associated with different Mn oxidation states.[18,19,37]

The Mn L-edge XA spectra of the MnP$_i$ modified BiVO$_4$ photoanode show two characteristic broad multiplet structures, L$_3$ and L$_2$ that are separated by spin-orbit coupling.[19] Since it shows the most pronounced changes under varying potential and illumination conditions, we restrict our analysis to the L$_3$-edge. The dotted vertical lines in Figure 3 indicate the peaks where major changes occur upon applying more positive potentials to the electrode. They correspond to different oxidation states of manganese in the oxides as discussed in detail in the literature.[19] We assign the spectral features at 640.6, 642.2 and 643.6 eV to contributions of Mn^{2+}, Mn^{3+} and Mn^{4+} oxidation states, respectively.[19] The sharp peak at 641.2eV is probably associated with birnessite. In addition, we observed a peak at 639.5 eV, which is most pronounced under dark conditions and is typical for Mn^{2+} in MnO (see Figure 3d and Table S1).

To display the spectral changes induced by different potentials and illumination conditions more clearly, the differences ($\Delta\mu$) between the spectra recorded at a certain potential under dark or light

conditions (μ) and the OCP under dark spectrum (μ_{OCP}) are shown at the bottom of each figure in Figure 3a-c. In the difference spectra, positive features imply increasing concentration of a specific Mn species while negative features imply decreasing concentration as compared to the concentration at OCP and dark. It can be seen that Mn species are oxidized during at sufficiently positive applied potentials. The Mn in the films is oxidized from 2^+ to 3^+ and 4^+, both in the dark and under illumination. Moreover, the difference spectra suggest a slightly larger concentration of $Mn^{3+,4+}$ species under illumination. The oxidation becomes more pronounced under illumination.

In order to get detailed electronic and structural information, linear combination fitting using the reference Mn L-edge spectra was carried out for different applied potentials. The linear combination fitting approach can provide quantitative information on oxidation states of the sample. It has been previously used, e.g., to analyze the electronic structure of other manganese oxide films in the literature.[18,19] Figure 4 shows an example of an experimental spectrum together with the best fit from a linear combination of the reference spectra in Figure 3d. In general, the experimental spectra were well reproduced by the linear combination fit. The slight mismatch is attributed to limited experimental resolution and/or incomplete representation of the sample spectra by the reference spectra (i.e., other Mn species or structures may also be present).[43] Table 1 shows the complete fitting results for the Mn L-edge spectra of our MnP$_i$ modified BiVO$_4$ photoanode under different conditions. It was found that a freshly prepared MnP$_i$-modified BiVO$_4$ photoanode at OCP under dark condition contains ~12 % of Mn^{2+}, 1% of Mn^{3+}, 14 % of $Mn^{3+,4+}$ and ~73% of Mn^{4+}. No or only negligible percentages of $Mn^{2+,3+}$ and a small amount of Mn^{3+} were found, which indicates that the electronic structure of the freshly prepared MnP$_i$ modified BiVO$_4$ is dominated by Mn^{4+}. From these results an average oxidation state of ~3.71 is determined for

OCP under dark condition. This average oxidation state is consistent with the previously obtained value by the coulometric titration method of 3.68.[22,23]
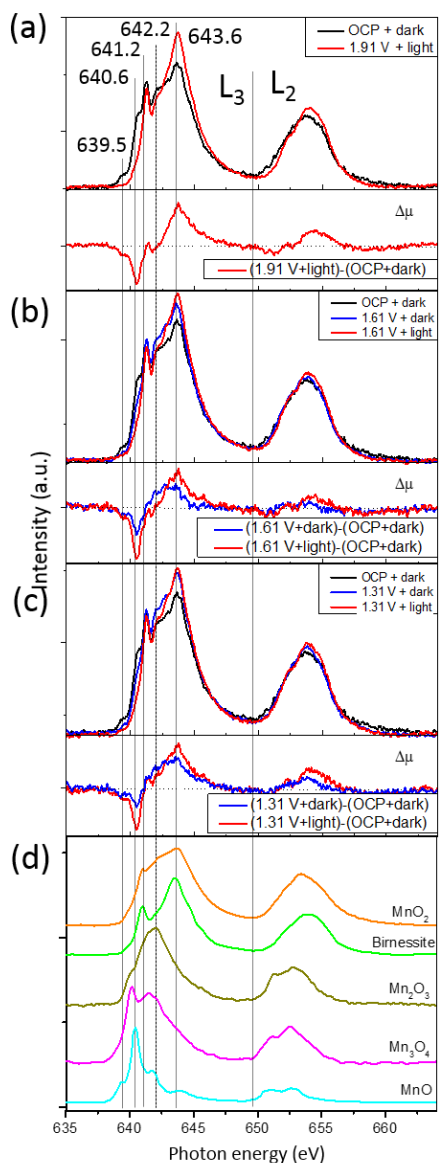

Figure 3. (a-c) In situ Mn L-edge spectra of a $MnP_i/BiVO_4/Au/Si_3N_4$ photoanode in 0.1 M KP_i buffer solution with 2.0 M KNO_3 added measured at different potentials and under illumination conditions. The test sequence is OCP, 1.91, 1.61 and 1.31 V, respectively, first under dark and then under illumination conditions. (d) The spectra of reference oxides are MnO,[37] Mn_2O_3, Mn_3O_4, birnessite and MnO_2.[18,19] The dotted lines are indicating the main peak positions of these oxides.
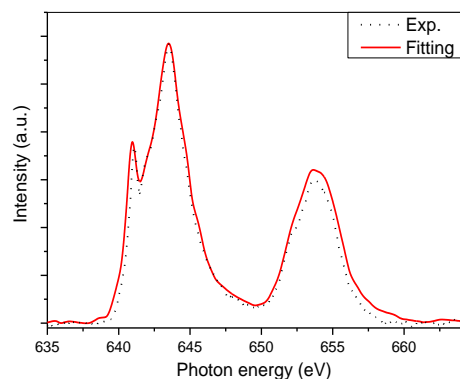
Figure 4. Experimental and fitted spectra for the spectrum at 1.91 V and under light.

Table 1. Summary of linear combination fitting of MnP$_i$ modified BiVO$_4$ photoanode under different potentials and light conditions. Here the average oxidation state of birnessite is taken as 3.7.36 Note: the test sequence is from the top to the bottom.

Potential (V)	MnO (2+) (%)	Mn$_3$O$_4$ (2+, 3+) (%)	Mn$_2$O$_3$ (3+) (%)	Birnessite (3+, 4+) (%)	MnO$_2$ (4+)(%)	Avg. oxid. State
OCP+dark	12	0	1	14	73	3.71
1.31+dark	0	0	13	36	51	3.76
1.31+light	0	0	11	60	29	3.71
1.61V+dark	0	0	14	44	42	3.73
1.61V+light	0	0	0	72	28	3.78
1.91V+light	0	0	0	82	18	3.75

When increasing the potential from OCP to 1.8 V, far above the thermodynamic value of water oxidation (1.23 V) under dark conditions, the average oxidation state of Mn from MnP$_i$ modified BiVO$_4$ photoanode does not significantly vary from OCP (3.71) to 1.31 V (3.76), then to 1.61 V (3.73) V in dark (also see Table 1). But the percentage of different Mn species varies a lot. For

example, at 1.3 V and light, there are 11% Mn^{3+}, 60% $Mn^{3+/4+}$ and 29% Mn^{4+}. At 1.61 V and light, there are 72% $Mn^{3+/4+}$ and 28% Mn^{4+}, but no Mn^{3+} species. In addition, we found there is a relaxation process. For example, compared to the spectra obtained at 1.31 V and light, Mn spectra obtained at 1.61 V and dark show a slow reduction process (see Figure S5). Our time-dependent studies at other potentials exclude the possibility of beam damage. It is clear that the effect of potential and light at the anode is accompanied with a change in the electronic structure of MnP_i as observable in the spectra of Figure 3a. Significant changes of the MnP_i L-edge spectra toward a further increase of the oxidation state of manganese ions in the catalyst become visible after illuminating the $BiVO_4$ layer and generating photoexcited holes (see peak at 643.6 eV indicating an increased Mn^{4+} concentration). This means that photogenerated holes in $BiVO_4$ are transferred to Mn sites further oxidizing MnP_i. In addition, comparing the shape of the L-edge spectrum at +1.91 V under illumination with the reference curves in Figure 3d the electrodeposited MnP_i appears to transform into a layered manganese oxide commonly known as birnessite (see increasing concentration of birnessite in Table 1). To enable this transformation, an uptake of potassium ions (K^+) from the buffer solution to form the KMn_8O_{16} phase between MnO_6 units is necessary. The higher activity towards OER at more positive potentials has previously been attributed to the upward band bending suppresses charge recombination and facilitates photoexcited hole transfer as reported in a previous works based on IR and TAS studies.[39-42] Our results suggest an alternative explanation, which is that the higher activity is simply caused by an increase in the birnessite content at these potentials. Various forms of birnessite are indeed known to be active OER catalysts[44] and we therefore propose that birnessite, not ordered MnO_2, is the active phase for the OER in MnP_i.

We further investigated the dynamics of the increase in Mn oxidation state in our MnP$_i$ modified BiVO$_4$. Figure 5 shows the temporal evolution of XA spectra of a MnP$_i$ modified BiVO$_4$ photoanode at OCP or 1.61 V, both under illumination. At OCP with increasing period of illumination (see Figure 5a), we can see that the intensity of the peak at 640.6 eV (Mn^{2+} species, peak position I) reduces and the intensities of peaks at 642.0 eV (Mn^{3+} species) and 643.6 eV (Mn^{4+}) increase (peak position III and V in Figure 5a). The intensity of peak at 642.7 eV (peak position IV) also increases. At this moment, it is unclear which Mn species it associates to. The intensity of peak at 640.6 eV (Mn^{2+} species, peak position I) keeps constant. The overall average oxidation state thus increases with time. This means that at OCP conditions, photo-generated holes oxidize MnP$_i$ even without any external potential. Ma *et al.*[45] found that the transient kinetics of the unbiased BiVO$_4$ film in the absence of scavengers is closest to that observed under modest anodic bias (~0.6V), indicative of the presence of band bending in the BiVO$_4$ electrode in water without any applied bias or scavengers. The OCP of the BiVO$_4$ photoanode in this study was measured to be around 0.58 V. Thus, we expected similar a band bending in our photoanodes. At 1.61 V and with increasing period of illumination (see Figure 5b), the intensities of peaks at arrow II, III and IV while the intensities at arrow I and V keep constant. With increasing potential, the course of the curve is approaching the features of the birnessite reference spectrum. At such positive potentials, the transfer rate of the photogenerated holes increases probably due to a reduction of electron/hole recombination losses.[45] This result implies that the electronic structure of the Mn species can be modified upon electron/hole migration between the BiVO$_4$ photoanode and the MnP$_i$ film. This time-dependent process can explain the so-called "activation process" proposed for the MnO$_x$ OER catalyst.[45] We confirmed that similar activation did not happen in the dark under the same potential (see Figure S5), due to the absence of hole transfer from the BiVO$_4$

photoanode toward the MnP$_i$ catalyst layer. The electronic structure changes of MnP$_i$ on our BiVO$_4$ photoanode after ~10 min are found to be larger than those observed in other reports on other MnO$_x$ in the literature. [39, 42] This suggests that MnP$_i$ is more active than these MnO$_x$ phases. Moreover, in those works, Yoshida *et al*. found that it took around 2 h to get stable MnO$_x$ on a Nb:SrTiO$_3$ photoelectrode under UV illumination. As proposed previously that the rate of structural change of the Mn oxidation correlates with the PEC activity,[39] our results indicate that the photogenerated holes in BiVO$_4$ are very efficiently transferred to the MnP$_i$.
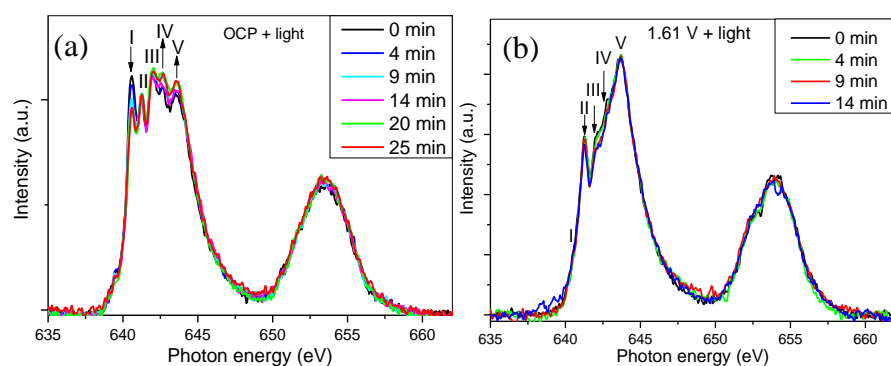

Figure 5. Temporal evolution of XA spectra of a MnP$_i$ modified BiVO$_4$/Au/Si$_3$N$_4$ photoanode in 0.1 M KP$_i$ buffer solution with KNO$_3$ added at: (a) OCP and (b) 1.61 V under light.

We note that our findings differ from an earlier study on MnO$_x$ clusters by Hocking *et al*.[21] They reported that MnO$_x$ had two chemical states: the electrochemically reduced Mn^{3+} (the reduced state) and the electrochemical oxidized Mn^{4+} (the oxidized state).[21] Both Mn^{3+} and Mn^{4+} oxides species are reported to function as water oxidation catalysts. In contrast to these investigated MnO$_x$ clusters, our soft XA spectra clearly showed that the MnP$_i$ films are different; it contains a mixture of Mn species. Table 1 and our results indicate that the main species during photoelectrochemical water oxidation are birnessite and MnO$_2$, and the amount of birnessite structure increases when applying high potential. Birnessite is composed of layers of edge-sharing MnO$_6$ octahedra with an interlayer of hydrated cations.[46,36] As cations, eg. K$^+$ or Ca^{2+}, are intercalated due to surface

17

adsorption, intercalation of electrolyte anions, and/or surface structure changes under electric field, manganese ions are converted from a stable d^3 (Mn^{4+}) state to an unstable high-spin d^4 state (Mn^{3+}). These Mn^{3+} cations will undergo a strong Jahn−Teller effect, elongating a pair of oxygens in order to split degenerate d orbitals to fill lower energy orbital.[46] Thus, the birnessite contains a majority of Mn^{4+} species and a minority of Mn^{3+} species. In the literature, the role of the Mn^{3+} species and the active site in birnessite have been well studied. For example, Takashima *et al.*[47] studied the catalytic properties of manganese oxide films and proposed that Mn^{3+} has a role in lowering the overpotential for electrochemical water oxidation on birnessite. They found that OER is enhanced in manganese oxides when Mn^{3+} is introduced through voltage cycling protocols or via chemical synthesis. This study strengthened the important role that Mn^{3+} on birnessite plays in facilitating OER. Smith *et al.* recently compared electrocatalytic performance of crystalline edge- vs corner-shared Mn^{3+} birnessite samples and found that the activity does not necessarily correlate with total Mn^{3+} content but, more likely, with the content of corner-shared Mn^{3+} sites.[48] McKendry *et al.* decorated the layered manganese oxide birnessite with Mn^{2+} and Mn^{3+} and attributed the catalytic activity of the birnessite to Mn^{3+}-based active sites.[49] Similar to the catalyst studied here, Huynh *et al.* proposed that Mn^{3+} sites are likely introduced when hausmannite (α-Mn_3O_4) is imperfectly converted to disordered birnessite.[23,24] The large structural change when transforming from a spinel (hausmannite) to a layered material (birnessite) is kinetically sluggish and may result in imperfections that trap Mn^{3+} species, which logically comprise the resting state of highly active sites for oxygen evolution. Based on our results and literature findings, we thus conclude that Mn^{3+} species, not Mn^{4+}, in birnessite is the active sites for oxygen evolution reaction. This means that in order to improve the catalytic performance of MnP_i itself or on $BiVO_4$ photoande, a conversion from the ordered MnO_2 to disordered birnessite phase is highly demanded. The amount of corner-

shared Mn^{3+} sites in birnessite should be increased because it is mostly a crucial part to achieving a high active manganese oxide OEC. *In situ* electronic structural study using soft XAS can help to monitor and design more effective semiconductor/catalyst systems. We further investigated the vanadium (V) L–edge of the $BiVO_4$ photoanodes under different potentials and light conditions (see Figure S6). It was found there is no change in the electronic structure of V under our test conditions. This is not surprising, since the oxidation state of V in $BiVO_4$ is already 5+.[50] This is the highest oxidation state of vanadium and thus insensible to external bias.

Based on our XAS results, we propose a schematic illustration of photogenerated carrier transfer from the $BiVO_4$ photoanode to the MnP_i film during PEC water oxidation at three conditions: 0.00 V, OCP and 1.61 V, as shown in Figure 6. When the electrode remains at the potential of 0.00 V, which is close to the flat band potential of $BiVO_4$ as proposed in the literature,[51] band bending does not occur at the $MnP_i/BiVO_4$ interface. Photoexcited holes therefore do not migrate to the MnP_i because of the absence of a driving force and only recombine with photogenerated electrons in the photoelectrode. This scenario is consistent with the negligible PEC activity in Figure 2. When switching to OCP condition (0.58 V in this study), a slightly upward band bending occurs at the $MnP_i/BiVO_4$ interface. This promotes charge separation and provides the driving force for the migration of photogenerated holes toward the MnO_x layer. Water oxidation, however, does not occur at this potential; majority of the photogenerated carriers will either accumulate and flatten the band, or recombine at the surface.[6] When applying potential of 1.61 V or higher, a further downward band bending at the $MnP_i/BiVO_4$ interface occurs. It strongly promotes charge separation and results in an efficient migration of photogenerated holes toward the MnP_i layer. This is consistent with the strong decrease in surface recombination at potentials >1.0 V recently observed by Zachäus *et al*., which was attributed to unpinning of the Fermi level in $BiVO_4$ at these

potentials.[6] Meanwhile, this bending helps electron to move through the BiVO$_4$ to the external circuit. The holes accumulated at the interface of MnP$_i$ do not only oxidize Mn but also water directly, especially at modest applied potentials. This is again consistent with the model of Zachäus *et al*.
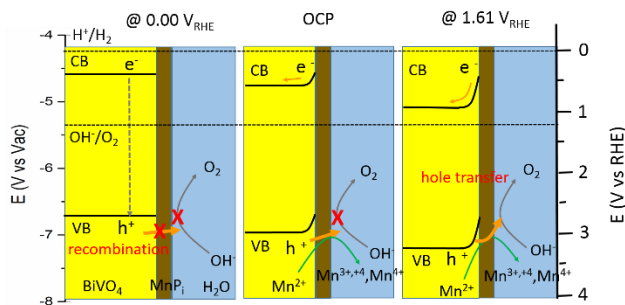

Figure 6. A schematic illustration of the photogenerated carrier transfer from the BiVO$_4$ photoanode to the MnP$_i$ film at 0.00 V, OCP condition and 1.61 V vs RHE.

CONCLUSION

In summary, we demonstrated that the PEC performance of a BiVO$_4$ photoanode can be improved by MnP$_i$ modification. The current density at 1.23 V of the pristine BiVO$_4$ is 0.48 mA cm^{-2} and increases to 0.62 mA cm^{-2} after MnP$_i$ modification (29% improvement). To investigate the electronic structure of a MnP$_i$ layer deposited on BiVO$_4$, in situ soft X-ray absorption spectroscopy was employed. The Mn L-edge spectra under different potentials and light conditions were investigated. Using the linear combination method, the information on the average oxidation state of Mn in the oxide as well as the percentage of different Mn species in the film under applied potential and illumination were revealed. We found that charge transfer of holes into the MnP$_i$ layer and to the electrolyte interface is occurring which is enhanced by a band bending in the semiconductor under illumination which is related to an increased potential by a built-in photopotential. We found that photo-generated holes can oxidize the MnPi layer even at OCP, i.e.,

without an external potential. With increasing potential the electronic structure of the MnO_x layer and its structure are changing to a birnessite-type layer structure associated with electron migration from the MnP_i film into the $BiVO_4$ photoanode. The formation of birnessite must be accompanied by the incorporation of K^+ between the MnO_6 layers, leading for example to a KMn_8O_{16} phase. Our results indicate that photogenerated holes are efficiently transferred to the MnP_i film. Based on the above results, a mechanism of the photogenerated carrier transfer from the $BiVO_4$ photoanode into the MnPi film at different potentials is proposed. Based on our results and literature findings, we conclude that Mn^{3+} species, not Mn^{4+}, in birnessite is the active sites for oxygen evolution reaction. *In situ* electronic structural study using soft XAS can help to monitor and design more effective semiconductor/catalyst systems.

ASSOCIATED CONTENT

SUPPORTING INFORMATION

The Supporting Information is available free of charge on the ACS Publications website at DOI:

Additional experimental, SEM images, additional XAS spectra, DEMS profiles and linear combination fitting calculations (PDF).

AUTHOR INFORMATION

Corresponding Author

kathrin.lange@helmholtz-berlin.de

Notes

The authors declare no competing financial interest.

ACKNOWLEDGMENTS

REFERENCES

(1) Walter, M. G.; Warren, E. L.; McKone, J. R.; Boettcher, S. W.; Mi, Q.; Santori, E. A.; Lewis, N. S. Solar Water Splitting Cells. *Chem. Rev.* **2010**, *110*, 6446-6473.

(2) Yang, J. H.; Wang, D. G.; Han, H. X.; Li, C. Roles of Cocatalysts in Photocatalysis and Photoelectrocatalysis. *Acc. Chem. Res.* **2013**, *46*, 1900-1909.

(3) Sivula, K.; Le Formal, F.; Gratzel, M. Solar Water Splitting: Progress Using Hematite (α-Fe_2O_3) Photoelectrodes. *ChemSusChem,* **2011**, *4*, 432-449.

(4) Sivula, K.; van de Krol, R. Semiconducting Materials for Photoelectrochemical Energy Conversion. *Nat. Rev. Mater.* **2016**, *1,* 15010.

(5) Trześniewsk, B. J.; Smith, W. A. Photocharged $BiVO_4$ Photoanodes for Improved Solar Water Splitting. *J. Mater. Chem. A* **2016**, *4*, 2919-2926.

(6) Zachäus, C.; Abdi, F. F.; Peter, L. M.; van de Krol, R. Photocurrent of $BiVO_4$ is Limited by Surface Recombination, Not Surface Catalysis. *Chem. Sci.* **2017**,*8,* 3712-3719.

(7) Jia, Q.; Iwashina, K.; Kudo, A. Facile Fabrication of an Efficient $BiVO_4$ Thin Film Electrode for Water Splitting under Visible Light Irradiation. *Proc. Natl. Acad. Sci. U. S. A.* **2012**, *109*, 11564-11569.

(8) Ding, C. M.; Shi, J. Y.; Wang, D. G.; Wang, Z. J.; Wang, N.; Liu, G. J.; Xiong, F. Q.; Li, C. Visible Light Driven Overall Water Splitting Using Cocatalyst/$BiVO_4$ Photoanode with Minimized Bias. *Phys. Chem. Chem. Phys.* **2013**, *15*, 4589-4595.

(9) Pilli, S. K.; Furtak, T. E.; Brown, L. D.; Deutsch, T. G.; Turner, J. A.; Herring, A. M. Cobalt-Phosphate (Co-P$_i$) Catalyst Modified Mo-doped BiVO$_4$ Photoelectrodes for Solar Water Oxidation. *Energy Environ. Sci.* **2011**, *4*, 5028– 5034.

(10) Abdi, F. F.; van de Krol, R. Nature and Light Dependence of Bulk Recombination in Co-Pi-Catalyzed BiVO4 Photoanodes. *J. Phys. Chem. C* **2012**, *116*, 9398-9404.

(11) Jeon, T. H.; Choi, W.; Park, H. Cobalt–Phosphate Complexes Catalyze the Photoelectrochemical Water Oxidation of BiVO$_4$ Electrodes. *Phys. Chem. Chem. Phys.* **2011**, *13,* 21392– 21401.

(12) Choi, S. K.; Choi, W.; Park, H. Solar Water Oxidation Using Nickel-Borate Coupled BiVO$_4$ Photoelectrodes. *Phys. Chem. Chem. Phys.* **2013**, *15*, 6499– 6507.

(13) Pilli, S. K.; Summers, K.; Chidambaram, D. Ni–Ci Oxygen Evolution Catalyst Integrated BiVO$_4$ Photoanodes for Solar Induced Water Oxidation. *RSC Adv.* **2015**, *5*, 47080-47089.

(14) Seabold, J. A.; Choi, K.-S. Efficient and Stable Photo-Oxidation of Water by a Bismuth Vanadate Photoanode Coupled with an Iron Oxyhydroxide Oxygen Evolution Catalyst. *J. Am. Chem. Soc.* **2012**, *134*, 2186-2192.

(15) Kim, T. W.; Choi, K.-S. Nanoporous BiVO$_4$ Photoanodes with Dual-Layer Oxygen Evolution Catalysts for Solar Water Splitting. *Science* **2014**, *343*, 990-994.

(16) Liang, Y.; Tsubota, T.; Mooij, L. P. A.; van de Krol, R. Highly Improved Quantum Efficiencies for Thin Film BiVO$_4$ Photoanodes. *J. Phys. Chem. C* **2011**, *115*, 17594-17598.

(17) Shi, X.; Zhang, K.; Shin, K.; Ma, M.; Kwon, J.; Choi, I. T.; Kim, J. K.; Kim, H. K.; Wang, D. H.; Park, J. H. Unassisted Photoelectrochemical Water Splitting beyond 5.7% Solar-to-Hydrogen Conversion Efficiency by a Wireless Monolithic Photoanode/Dye-Sensitised Solar Cell Tandem Device. *Nano Energy* **2015**, *13*, 182-191.

(18) Khan, M.; Xiao, J.; Zhou, F.; Yablonskikh, M.; MacFarlane, D. R.; Spiccia, L.; Aziz, E. F. On the Origin of the Improvement of Electrodeposited MnO_x Films in Water Oxidation Catalysis Induced by Heat Treatment. *ChemSusChem* **2015**, *8*, 11, 1980-1985.

(19) Khan, M.; Suljoti, E.; Singh, A.; Bonke, S. A.; Brandenburg, T.; Atak, K.; Golnak, R.: Spiccia, L.; Aziz, E. F. Electronic Structural Insights into Efficient MnO_x Catalysts. *J. Mater. Chem. A* **2014**, *2*, 18199-18203.

(20) Najafpour, M. M.; Moghaddam, A. N. Nano-Sized Manganese Oxide: a Proposed Catalyst for Water Oxidation in the Reaction of Some Manganese Complexes and Cerium (IV) Ammonium Nitrate. *Dalton Trans.* **2012**, *41*, 10292-10297.

(21) R. K. Hocking, R. Brimblecombe, L.-Y. Chang, A. Singh, M. H. Cheah, C. Glover, W. H. Casey and L. Spiccia, Water-Oxidation Catalysis by Manganese in a Geochemical-Like Cycle. *Nat. Chem.* **2011**, *3*, 461-466.

(22) Huynh, M.; Bediako, D. K.; Liu, Y.; Nocera, D. G. Nucleation and Growth Mechanisms of an Electrodeposited Manganese Oxide Oxygen Evolution Catalyst. *J. Phys. Chem. C* **2014**, *118*, 17142–17152.

(23) Huynh,M.; Shi, C.; Billinge, S.J.; Nocera, D.G. Nature of Activated Manganese Oxide for Oxygen Evolution. *J. Am. Chem. Soc.* **2015**, *137*, 14887-14904.

(24) Huynh, M.; Bediako, D. K.; Nocera, D. G A Functionally Stable Manganese Oxide Oxygen Evolution Catalyst in Acid. *J. Am. Chem. Soc.* **2014**, *136*, 6002-6010.

(25) Lange, K. M.; Kothe, A.; Aziz, E. F. Chemistry in Solution: Recent Techniques and Applications Using Soft X-ray Spectroscopy. *Phys. Chem. Chem. Phys*. **2012**, *14*, 5331-5338.

(26) Lange, K. M.; Aziz, E. F. Electronic Structure of Ions and Molecules in Solution: a View from Modern Soft X-ray Spectroscopies. *Chem. Soc. Rev*. **2013**, *42*, 6840-6859.

(27) Mierwaldt, D.; Mildner, S.; Arrigo, R.; Knop-Gericke, A.; Franke, E.; Blumenstein, A.; Hoffmann, J.; Jooss, C. In Situ XANES/XPS Investigation of Doped Manganese Perovskite Catalysts. *Catalysts* **2014**, *4*, 129–145.

(28) Pickrahn, K. L.; Gorlin, Y.; Seitz, L. C.; Garg, A.; Nordlund, D.; Jaramillo, T. F.; Bent, S. F. Applications of ALD MnO to Electrochemical Water Splitting. *Phys. Chem. Chem. Phys.* **2015**, *17*, 14003-14011.

(29) Cramer, S. P.; de Groot, F. M. F.; Ma, Y. J.; Chen, C. T.; Sette, F.; Kipke, C. A.; Eichhorn, D. M.; Chan, M. K.; Armstrong, W. H.; Libby, E. et al. Ligand Field Strengths and Oxidation States from Manganese L-edge Spectroscopy. *J. Am. Chem. Soc.* **1991**, *113,* 7937-7940.

(30) Axnanda, S.; Crumlin, E. J.; Mao, B.; Rani, S.; Chang, R.; Karlsson, P. G.; Edwards, M. O. M.; Lundqvist, M.; Moberg, R.; Ross, P. Using "Tender" X-ray Ambient Pressure X-Ray Photoelectron Spectroscopy as A Direct Probe of Solid-Liquid Interface. *Sci. Rep.* **2015**, *5*, 9788.

(31) Xi, L.F.; Schwanke, C.;Xiao, J.; Abdi, F.F.; Lange, K. M. In Situ L-edge XAS Study of a Manganese Oxide Water Oxidation Catalyst. *J. Phys. Chem. C.* **2017**, *121,* 12003-12009.

(32) Schwanke, C.; Xi, L.; Lange, K. M. A soft XAS Transmission Cell for Operando Studies. *J. Synchrotron Rad.* **2016**, *23*, 1390-1394.

(33) Gong, H.; Freudenberg, N.; Nie, M.; Van de Krol, R.; Ellmer, K. $BiVO_4$ Photoanodes For Water Splitting with High Injection Efficiency Deposited by Reactive Magnetron Co-Sputtering. *AIP Adv.* **2016**, *6,* 045108.

(34) Bogdanoff, P.; Alonso-Vante, N. A Kinetic Approach of Competitive Photoelectrooxidation of HCOOH and H_2O on TiO_2 Anatase Thin Layers via On-Line Mass Detection. *J. Electroanal. Chem.* **1994**, *379*, 415-421.

(35) Bogdanoff, P.; Alonso-Vante,N.; On-line Determination via Differential Electrochemical Mass Spectroscopy (DEMS) of Chemical Products Formed in Photoelectrocatalytical Systems. *Ber. Bunsen-Ges. Phys. Chem.* **1993***, 97*, 940-942.

(36) Golden, D. C.; Dixon J. B.; Chen, C. C. Ion Exchange, Thermal Transformations, and Oxidizing Properties of Birnessite. *Clays Clay Miner.* **1986***, 34*, 511-520.

(37) Qiao, R.; Chin, T.; Harris, S. J.; Yan, S.; Yang, W.L. Spectroscopic Fingerprints of Valence and Spin States in Manganese Oxides and Fluorides. *Curr. Appl. Phys.* **2013***, 13*, 544-548.

(38) Ching, S.; Petrovay, D. J.; Jorgensen, M. L.; Suib, S. L. Sol−Gel Synthesis of Layered Birnessite-Type Manganese Oxides. *Inorg. Chem.* **1997***, 36*, 883-890.

(39) Yoshida, M.; Yomogida, T.; Mineo, T.; Nitta, K.; Kato, K.; Masuda, T.; Nitani, H.; Abe, H.; Takakusagi, S.; Uruga, T. Photoexcited Hole Transfer to a MnO_x Cocatalyst on a $SrTiO_3$ Photoelectrode during Oxygen Evolution Studied by In Situ X-ray Absorption Spectroscopy. *J. Phys. Chem. C* **2014***, 118,* 24302-24309.

(40) Pendlebury, S. R.; Cowan, A. J.; Barroso, M.; Sivula, K.; Ye, J.; Grätzel, M.; Klug, D. R.; Tang, J.; Durrant, J. R. Correlating Long-Lived Photogenerated Hole Populations with Photocurrent Densities in Hematite Water Oxidation Photoanodes. *Energy Environ. Sci.* **2012***, 5,* 6304-6312.

(41) Yamakata, A.; Yoshida, M.; Kubota, J.; Osawa, M.; Domen, K. Potential-Dependent Recombination Kinetics of Photogenerated Electrons in n- and p-type GaN Photoelectrodes Studied by Time-Resolved IR Absorption Spectroscopy. *J. Am. Chem. Soc.* **2011***, 133,* 11351-11357.

(42) Yoshida, M.; Yomogida, T.; Mineo, T.; Nitta, K.; Kato, K.; Masuda, T.; Nitani, H.; Abe, H.; Takakusagi, S.; Uruga, T. In Situ Observation of Carrier Transfer in the Mn-oxide/Nb:SrTiO$_3$ Photoelectrode by X-ray Absorption Spectroscopy. *Chem. Commun.* **2013**, *49*, 7848-7850.

(43) Datta, S.; Rule, A. M.; Mihalic, J. N.; Chillrud, S. N.; Bostick, B. C.; Ramos-Bonilla, J. P.; Han, I.; Polyak, L. M.; Geyh, A. S.; Breysse, P. N. Use of X-ray Absorption Spectroscopy To Speciate Manganese in Airborne Particulate Matter from Five Counties Across the United States. *Environ. Sci. Technol.* **2012**, *46*, 3101-3109.

(44) Wiechen, M.; Zaharieva, I.; Dau, H.; Kurz, P. Layered Manganese Oxides for Water-Oxidation: Alkaline Earth Cations Influence Catalytic Activity in a Photosystem II-Like Fashion. *Chem. Sci.* **2012**, *3*, 2330-2339.

(45) Ma, Y.; Pendlebury, S. R.; Reynal, A.; Le Formal, F.; Durrant, J. R. Dynamics of Photogenerated Holes in Undoped BiVO$_4$ Photoanodes for Solar Water Oxidation. *Chem. Sci.* **2014**, *5*, 2964-2973.

(46) Lucht, K. P.; Mendoza-Cortes, J. L. Birnessite: A Layered Manganese Oxide To Capture Sunlight for Water-Splitting Catalysis. *J. Phys. Chem. C* **2015**, *119*, 22838−22846.

(47) Takashima, T.; Hashimoto, K.; Nakamura, R. Inhibition of Charge Disproportionation of MnO$_2$ Electrocatalysts for Efficient Water Oxidation under Neutral Conditions. *J. Am. Chem. Soc.* **2012**, *134*, 18153-18156.

(48) Smith, P. F.; Deibert, B. J.; Kaushik, S.; Gardner, G.; Hwang, S.; Wang, H.; Al-Sharab, J. F.; Garfunkel, E.; Fabris, L.; Li, J.; Dismukes, C. Coordination Geometry and Oxidation State Requirements of Corner-Sharing MnO$_6$ Octahedra for Water Oxidation Catalysis: An Investigation of Manganite (γ-MnOOH). ACS Catal. 2016, 6, 2089-2099.

(49) McKendry, I. G.; Kondaveeti, S. K.; Shumlas, S. L.; Strongin, D. R.; Zdilla, M. J. Decoration of the Layered Manganese Oxide Birnessite with Mn(II/III) Gives a New Water Oxidation Catalyst with Fifty-Fold Turnover Number Enhancement. Dalt. Trans. 2015, 44, 12981-12984.

(50) Berglund, S. P.; Flaherty, D. W.; Hahn, N. T.; Bard, A. J.; Mullins, C. B. Photoelectrochemical Oxidation of Water Using Nanostructured $BiVO_4$ Films. *J. Phys. Chem. C* **2011***, 115*, 3794-3802.

(51) Sayama, K.; Nomura, A.; Arai, T.; Sugita, T.; Abe, R.; Yanagida, M.; Oi, T.; Iwasaki, Y.; Abe, Y.; Sugihara, H. Photoelectrochemical Decomposition of Water into H_2 and O_2 on Porous $BiVO_4$ Thin-Film Electrodes under Visible Light and Significant Effect of Ag Ion Treatment. *J. Phys. Chem. B* **2006***, 110*, 11352-11360.

TOC Graphic